Fundamental limits to attractive and repulsive Casimir-Polder forces

Prashanth S. Venkataram, Sean Molesky, Pengning Chao ⬤, and Alejandro W. Rodriguez
Department of Electrical Engineering, Princeton University, Princeton, New Jersey 08544, USA

We derive upper and lower bounds on the Casimir-Polder force between an anisotropic dipolar body and a macroscopic body, separated by vacuum, via algebraic properties of Maxwell's equations. These bounds require only a coarse characterization of the system—the material composition of the macroscopic object, the polarizability of the dipole, and any convenient partition between the two objects—to encompass all structuring possibilities. We find that the attractive Casimir-Polder force between a polarizable dipole and a uniform planar semi-infinite bulk medium always comes within 10% of the lower bound, implying that nanostructuring is of limited use for increasing attraction. In contrast, the possibility of repulsion is observed even for isotropic dipoles, and is routinely found to be several orders of magnitude larger than any known design, including recently predicted geometries involving conductors with sharp edges. These results may have ramifications for the design of surfaces to trap, suspend, or adsorb ultracold gases.

I. INTRODUCTION

Casimir forces between polarizable bodies arise from zero-point fluctuations of the electromagnetic (EM) field [1–11]. Commonly, the interaction is named "Casimir" for forces between larger bodies (modeled with continuum susceptibilities) at length scales where EM retardation is relevant, "van der Waals" (vdW) when EM retardation can be ignored but atom-scale features cannot, and "Casimir-Polder" (CP) when EM retardation is relevant but at least one of the bodies can be approximated as dipolar. Over the past decade, improved experimental techniques have allowed the characteristics of all three regimes to be examined with consistently increasing accuracy. vdW forces at small separations ($\lesssim 10$ nm) between bodies with atomically small dimensions have been measured with molecules, macromolecular arrays, single-layer sheets, and planar metallic or dielectric substrates without EM retardation [12–14], as well as those between nanoparticles and nanotubes [15,16]. CP forces have been experimentally measured in systems including planar substrates, gratings, Rydberg atoms, molecules, and Bose-Einstein condensates [1–4,12,17,18]. Casimir forces have been measured in both vacuum [19–22] and fluid media [23,24].

In tandem, there is mounting interest in exploring how complex nanostructured geometries [8,25–27], such as interleaved gratings, can be used to alter the magnitude as well as the sign of these forces compared to typical attractive Casimir forces, which monotonically decay as a power law with respect to separation for planar media [1–3,5,28]. Potential applications exist over a broad range of length scales. Following the finding that vdW interactions at the molecular scale can significantly affect predicted material stability and mechanical properties [8,29–32], atomic-scale vdW forces in materials like graphene, phosphorene, proteins, nanotubes, and fullerenes may lead to novel biological sensors and techniques for tailoring nanoscale self-assembly [10,11,33,34]. Casimir interactions among larger bodies may be exploited to engineer future microelectrome-chanical systems [26,27,35,36], mechanisms for stabilizing nanoscale objects in fluids [23,24], and methods for overcoming "stiction" in microchips [35,37]. Structuring large substrates to tailor CP interactions could provide refined spatial control over ultracold ground-state or Rydberg atoms, molecules, or quantum emitters [1–3,17,18,38–40].

Moreover, there is fundamental interest in understanding the asymmetry of Casimir interactions. Repulsive Casimir forces have been experimentally observed in systems satisfying the Dzyaloshinskii-Lifshitz-Pitaevskii permittivity criterion for repulsion [23,24,41–43], requiring an intervening medium such as a fluid, for more than a decade. However, for systems in vacuum, to the best of our knowledge, repulsive Casimir and CP forces have only been theoretically predicted in a few special systems, such as strongly anisotropic dipoles at small separations [44,45], planar magnetic media [43,46–48], metallic rectangular gratings [40], metallic or dielectric plates with circular holes [44,49,50], and other metallic surfaces with sharp edges [51,52]. Due to the extremely weak forces involved, the magnetic response or dipolar anisotropies involved would have to be unphysically large for these proposals to produce repulsive Casimir or CP forces in vacuum measurable with current techniques.

There is, presently, no formally established proof that CP repulsion must be so weak (i.e., that substantially stronger CP attraction is not possible). General bounds on Casimir forces in arbitrary geometries have been broadly restricted to qualitative "yes or no" statements, such as the no-go theorem for repulsion in mirror-symmetric systems in vacuum [53] and generalizations of Earnshaw's theorem for setting constraints on stable equilibria [54]. Quantitative limits on force magnitude have been deduced almost exclusively for uniform planar dielectric and magnetic media [55,56] and have not been generalized to arbitrary geometries.

In this paper, we present upper and lower bounds on CP forces for a dipolar body separated by vacuum from a macroscopic body of uniform susceptibility. These limits,
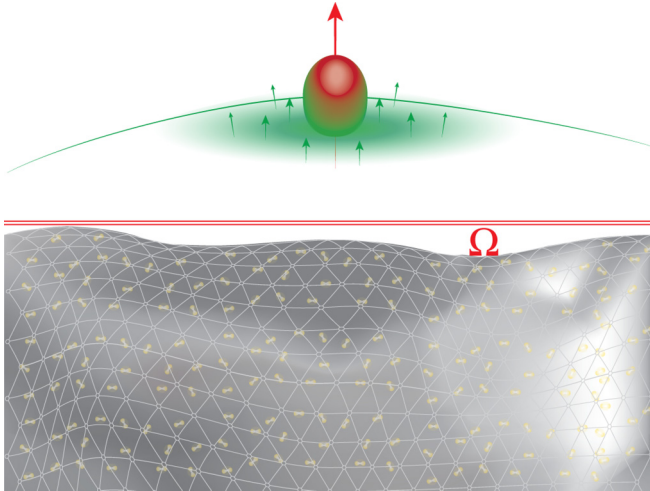
FIG. 1. Schematic of investigation. We derive shape-independent upper and lower bounds on the Casimir-Polder force between a polarizable dipolar body of parallel (perpendicular) polarizability $\alpha_\parallel$ ($\alpha_\perp$) above any nanostructured medium of susceptibility χ within a given domain Ω.

derived via Lagrange duality, depend only on the dipole polarizability, the susceptibility of the macroscopic body, and the choice of a partition separating the two objects (with positive bounds corresponding to repulsion and negative bounds to attraction), depicted schematically in Fig. 1. Surprisingly, these simple properties capture sufficient physics for seemingly plausible bounds. Regardless of anisotropy, the archetypal vertical CP force between a dipole and a semi-infinite planar bulk is consistently within 10% of the lower bound; thus, for attraction, the bound is relatively tight and nanostructuring can offer only modest improvements. Conversely, sharp contrasts between the bounds and known designs are observed for repulsive vertical forces. Irrespective of the polarizability of the dipolar body, repulsion is never completely ruled out, and in most cases the bound is found to be several orders of magnitude larger than what has been observed in any known design, including recently proposed (experimentally challenging) special geometries involving highly anisotropic dipolar bodies and metals with sharp edges [44,49,50]. This suggests that nontrivial nanostructuring may yet lead to feasible designs with strong (measurable) repulsive CP forces, of interest for controlling ultracold atomic gases and nanoparticles.

The text is laid out as follows. Our reasoning for the existence of the bounds described above, valid for any partition (domain) separating the dipole and the macroscopic body, is given in Sec. III. We provide this derivation in the main text so that interested readers may potentially use similar methods to extend this work to bounds on other EM phenomena. However, as the involved arguments are somewhat technical, prior to this discussion we simply state what will be shown in Sec. II, for readers primarily interested in application, physical intuition, and ramifications. In Sec. IV, we consider application of these general CP force limits to the vertical forces exerted by structures contained within a planar semi-infinite half-space. This example encompasses a very wide variety of possible compact and extended structure designs,

but by no means represents the full extent of the theory. Bounds on lateral CP forces, CP torques, and CP forces along other constrained paths are equally possible to evaluate using our results.

As notation, a vector field $\mathbf{v}(\mathbf{x})$ will be denoted as $|\mathbf{v}\rangle$. At $\omega = i\xi$, all relevant polarization and field quantities can be defined to be real valued in position space without loss of generality, so we define the *unconjugated* inner product $\langle \mathbf{u}, \mathbf{v} \rangle = \int d^3x\, \mathbf{u}(\mathbf{x}) \cdot \mathbf{v}(\mathbf{x})$. An operator $\mathbb{A}(\mathbf{x}, \mathbf{x}')$ will be denoted as $\mathbb{A}$, with $\int d^3x' \mathbb{A}(\mathbf{x}, \mathbf{x}') \cdot \mathbf{v}(\mathbf{x}')$ denoted as $\mathbb{A}|\mathbf{v}\rangle$. Unless stated otherwise, all quantities are taken to implicitly depend on $i\xi$. All results found in the main text are for zero temperature; results at nonzero temperature, particularly room temperature ($T = 300\,\mathrm{K}$), obtained through the Matsubara summation procedure [2,3], are discussed in Appendix C.

II. MAIN RESULT

Consider the CP force on a dipole of susceptibility $\mathbb{V}_{\mathrm{dip}}$. Correcting for local field effects (particularly important for dipolar metallic nanoparticles) requires use of the dressed response $\mathbb{T}_{\mathrm{dip}} = (\mathbb{V}_{\mathrm{dip}}^{-1} - \mathbb{G}^{\mathrm{vac}})^{-1} = (\mathbb{I} - \mathbb{V}_{\mathrm{dip}}\mathbb{G}^{\mathrm{vac}})^{-1}\mathbb{V}_{\mathrm{dip}}$ [57,58]. The dressed dipolar response may be expanded as $\mathbb{T}_{\mathrm{dip}} = \sum_\beta \alpha_\beta |\mathbf{u}^{(\beta)}\rangle \langle \mathbf{u}^{(\beta)}|$, where the polarizabilities $\alpha_\beta(i\xi)$ are positive and the basis functions $\mathbf{u}^{(\beta)}(\mathbf{x}) = \mathbf{n}_\beta \delta^3(\mathbf{x} - \mathbf{R})$ are given in terms of the dipole location $\mathbf{R}$ and the principal axes $\mathbf{n}_\beta$.

The upper and lower bounds (repulsion and attraction) on the CP force along Cartesian axis k, respectively F_k^+ and F_k^-, are shown to depend on $\mathbb{T}_{\mathrm{dip}}$, the macroscopic susceptibility $\chi(i\xi)$ (assumed to be homogeneous, local, and isotropic), and the choice of domain Ω enclosing the macroscopic body, all of which are completely general and independent of any particular material dispersion model or body shapes. As argued in the following derivation, the lower bounds can never increase, and the upper bounds never decrease, when the chosen domain Ω is enlarged, so that as a whole the bounds are domain monotonic. Based on this fact, the bounds on the CP force can be written at zero temperature as

$$F_k^\pm = \frac{\hbar}{2\pi} \int_0^\infty \sum_\beta \alpha_\beta \left[\left\langle \frac{\partial \mathbf{u}^{(\beta)}}{\partial R_k}, \mathbb{G}^{\mathrm{sca}}(\Omega)\mathbf{u}^{(\beta)} \right\rangle \right.$$
$$\left. \pm \left(\langle \mathbf{u}^{(\beta)}, \mathbb{G}^{\mathrm{sca}}(\Omega)\mathbf{u}^{(\beta)} \rangle \left\langle \frac{\partial \mathbf{u}^{(\beta)}}{\partial R_k}, \mathbb{G}^{\mathrm{sca}}(\Omega)\frac{\partial \mathbf{u}^{(\beta)}}{\partial R_k} \right\rangle \right)^{1/2} \right] d\xi,$$
$$(1)$$

where again all quantities are evaluated at $\omega = i\xi$; the derivation of these bounds is in the following section but is not needed to evaluate or understand the implications of these bounds. Here, $\mathbb{G}^{\mathrm{sca}}(\Omega)$ is the scattering Green's function of the equivalent object created by filling the chosen domain Ω *uniformly* with a material of susceptibility $\chi(i\xi)$, and *not* the scattering Green's function of any specific object possibly contained within the domain. [Crucially, (1) is not the expression of the CP force for any particular geometry.] These bounds need not have a definite sign either: For combinations of dipole polarizability $\{\alpha_\beta(i\xi)\}$, position $\mathbf{R}$, and domain choice Ω where the upper bound is positive and the lower

bound is negative, there are potentially structures producing either attractive or repulsive CP forces.

III. TECHNICAL DERIVATION

The actual CP force by a macroscopic body of susceptibility $\mathbb{V}$ on a dipole of susceptibility $\mathbb{V}_{\text{dip}}$ as above is written as

$$F_k = \frac{\hbar}{2\pi} \int_0^\infty \sum_\beta \alpha_\beta \frac{\partial}{\partial R_k} \langle \mathbf{u}^{(\beta)}, \mathbb{G}^{\text{vac}} \mathbb{T}(\mathbb{V}) \mathbb{G}^{\text{vac}} \mathbf{u}^{(\beta)} \rangle \, d\xi, \quad (2)$$

where $\mathbb{T}(\mathbb{V}) = [\mathbb{P}(\mathbb{V}) - \mathbb{V}\mathbb{G}^{\text{vac}}]^{-1}\mathbb{V}$ for the macroscopic body, which has the same support as $\mathbb{V}$ [denoted by the orthogonal projection operator $\mathbb{P}(\mathbb{V})$] and satisfies $\mathbb{T}(\mathbb{V}) = \mathbb{T}(\mathbb{V})[\mathbb{V}^{-1} - \mathbb{P}(\Omega)\mathbb{G}^{\text{vac}}\mathbb{P}(\Omega)]\mathbb{T}(\mathbb{V})$, $\mathbb{G}^{\text{vac}}$ is implicitly projected onto a domain Ω [denoted by the orthogonal projection operator $\mathbb{P}(\Omega)$] which contains the support of $\mathbb{V}$, and all quantities are evaluated at $\omega = i\xi$. We note that the formula for $\mathbb{T}$ arises from standard EM scattering theory [57,58] formulated as a Lippmann-Schwinger equation [59], and while we leave a derivation of the CP force formula to Appendix B, we point out that the actual CP force may be written more simply in terms of the scattering Green's function $\mathbb{G}^{\text{sca}}(\mathbb{V}) = \mathbb{G}^{\text{vac}}\mathbb{T}(\mathbb{V})\mathbb{G}^{\text{vac}}$ of a particular macroscopic object with susceptibility $\mathbb{V}$ (as writing it in this form is more typical of prior work on CP forces [1–3,5,28]). Henceforth, we assume that $\mathbb{V}$ represents a scalar (homogeneous, local, isotropic) susceptibility χ. Our goal then is to find bounds such that $F_k \in [F_k^-, F_k^+]$. We note that at $\omega = i\xi$, $\mathbb{V}$, $\mathbb{G}^{\text{vac}}$, and $\mathbb{T}$ in general are real-symmetric operators in position space, with $\mathbb{V}$ and $\mathbb{T}$ being positive definite while $\mathbb{G}^{\text{vac}}$ is negative definite (and this applies to its diagonal projected blocks too). Our derivations are based on analytical optimization using the principles of Lagrange duality, incorporating physical constraints imposed by $\mathbb{T}$; similar techniques have recently been used to derive bounds on deterministic EM scattering phenomena [60].

We first consider the problem of optimizing $\frac{\partial}{\partial R_k} \langle \mathbf{E}^{\text{inc}}, \mathbb{T}(\mathbb{V})\mathbf{E}^{\text{inc}} \rangle = 2\langle \frac{\partial \mathbf{E}^{\text{inc}}}{\partial R_k}, \mathbb{T}\mathbf{E}^{\text{inc}} \rangle$ for an arbitrary incident field $|\mathbf{E}^{\text{inc}}\rangle$. In particular, we define the action of $\mathbb{T}(\mathbb{V})$ to be a new vector $|\mathbf{P}\rangle = \mathbb{T}(\mathbb{V})|\mathbf{E}^{\text{inc}}\rangle$ and optimize the quantity $2\langle \frac{\partial \mathbf{E}^{\text{inc}}}{\partial R_k}, \mathbf{P} \rangle$ with respect to $|\mathbf{P}\rangle$, assuming that the response $|\mathbf{P}\rangle$ can be chosen arbitrarily given its support. However, we also take care to impose the equality constraint, which for a homogeneous local isotropic susceptibility χ may be rewritten as $\mathbb{T}(\mathbb{V}) = \mathbb{T}(\mathbb{V})[\chi^{-1}\mathbb{P}(\Omega) - \mathbb{P}(\Omega)\mathbb{G}^{\text{vac}}\mathbb{P}(\Omega)]\mathbb{T}(\mathbb{V})$ because the replacement of $\mathbb{V}^{-1} = \chi^{-1}\mathbb{P}(\mathbb{V})$ in the middle term in the product by $\chi^{-1}\mathbb{P}(\Omega)$ is allowed as the support of $\mathbb{T}(\mathbb{V})$ coincides with that of $\mathbb{V}$ and is in turn always a

weak subset of Ω. The equality constraint ensures physical consistency, and evaluating this with respect to $|\mathbf{E}^{\text{inc}}\rangle$ gives $\langle \mathbf{E}^{\text{inc}}, \mathbf{P} \rangle = \chi^{-1}\langle \mathbf{P}, \mathbf{P} \rangle - \langle \mathbf{P}, \mathbb{G}^{\text{vac}}\mathbf{P} \rangle$, which is positive as $\mathbb{T}$ is positive definite. For convenience, we define the eigenvalue decomposition of the projection of $\mathbb{G}^{\text{vac}}$ into the given domain Ω as $\mathbb{P}(\Omega)\mathbb{G}^{\text{vac}}\mathbb{P}(\Omega) = -\sum_\mu \rho_\mu |\mathbf{N}^{(\mu)}\rangle\langle\mathbf{N}^{(\mu)}|$, where $\rho_\mu > 0$, and the eigenvectors are orthonormal: $\langle \mathbf{N}^{(\mu)}, \mathbf{N}^{(\nu)} \rangle = \delta_{\mu\nu}$. We then define the basis expansions $v_\mu = \langle \mathbf{N}^{(\mu)}, \mathbf{E}^{\text{inc}} \rangle = \langle \mathbf{E}^{\text{inc}}, \mathbf{N}^{(\mu)} \rangle$ and $t_\mu = \langle \mathbf{N}^{(\mu)}, \mathbf{P} \rangle = \langle \mathbf{P}, \mathbf{N}^{(\mu)} \rangle$. As the domain choice is independent of $\mathbf{R}$, then $2\langle \frac{\partial \mathbf{E}^{\text{inc}}}{\partial R_k}, \mathbf{P} \rangle = 2\sum_\mu \frac{\partial v_\mu}{\partial R_k} t_\mu$. This leads to the constrained optimization of the objective

$$L = \sum_\mu \left\{ 2\frac{\partial v_\mu}{\partial R_k} t_\mu - \lambda[t_\mu v_\mu - (\chi^{-1} + \rho_\mu)t_\mu^2] \right\}, \quad (3)$$

where λ is a Lagrange multiplier.

We prove domain monotonicity of our bounds as follows. The support of $|\mathbf{P}\rangle$, encoded in the expansion coefficients $\{t_\mu\}$, is a subset of the domain Ω into which we choose to project $\mathbb{G}^{\text{vac}}$. Enlarging the domain Ω cannot affect the equality constraint, because the equality constraint involves the operator $\mathbb{T}(\mathbb{V})$ that is supported in this subset of Ω, so any enlargement of the domain Ω will ultimately be collapsed to the smaller support of the operator $\mathbb{T}(\mathbb{V})$. Similarly, the magnitude of the bound cannot decrease with increasing domain Ω, because the expansion coefficients $\{t_\mu\}$ representing $|\mathbf{P}\rangle$ can always be chosen to remain unchanged with an increasing domain Ω, given that the objective collapses onto the smaller domain (the support of $|\mathbf{P}\rangle$) anyway. Thus, our bound is domain monotonic, and so any domain with projection operator $\mathbb{P}(\Omega)$ that fully encloses all possible object designs of interest can be used to generate bounds: Put simply, any optimal design for attraction or repulsion in a given domain cannot outdo the corresponding optimal design from a superset of that domain.

Carrying out the optimization yields the equations $2\frac{\partial v_\mu}{\partial R_k} - \lambda[v_\mu - 2(\chi^{-1} + \rho_\mu)t_\mu] = 0$ and $\sum_\mu [t_\mu v_\mu - (\chi^{-1} + \rho_\mu)t_\mu^2] = 0$. The first equation gives $t_\mu = \frac{1}{\chi^{-1} + \rho_\mu}(\frac{v_\mu}{2} - \frac{1}{\lambda}\frac{\partial v_\mu}{\partial R_k})$, and plugging this into the second equation gives

$$\lambda \in \pm 2\sqrt{\frac{\langle \frac{\partial \mathbf{E}^{\text{inc}}}{\partial R_k}, [\chi^{-1}\mathbb{P}(\Omega) - \mathbb{P}(\Omega)\mathbb{G}^{\text{vac}}\mathbb{P}(\Omega)]^{-1}\frac{\partial \mathbf{E}^{\text{inc}}}{\partial R_k}\rangle}{\langle \mathbf{E}^{\text{inc}}, [\chi^{-1}\mathbb{P}(\Omega) - \mathbb{P}(\Omega)\mathbb{G}^{\text{vac}}\mathbb{P}(\Omega)]^{-1}\mathbf{E}^{\text{inc}}\rangle}}.$$

The constrained objective has $\frac{\delta^2 L}{\delta t_\mu \delta t_\nu} = 2\lambda(\chi^{-1} + \rho_\mu)\delta_{\mu\nu}$, so the negative value of λ gives the maximum while the positive value gives the minimum. (Another special stationary point corresponding to $\lambda = 0$, which is a saddle point, can be found if $|\frac{\partial \mathbf{E}^{\text{inc}}}{\partial R_k}\rangle = 0$; this cannot arise for the incident field radiated by a dipole into a domain, so we do not consider it further.) Hence, $L \in [L^-, L^+]$, with

$$L^\pm = \left\langle \frac{\partial \mathbf{E}^{\text{inc}}}{\partial R_k}, [\chi^{-1}\mathbb{P}(\Omega) - \mathbb{P}(\Omega)\mathbb{G}^{\text{vac}}\mathbb{P}(\Omega)]^{-1}\mathbf{E}^{\text{inc}} \right\rangle$$

$$\pm \sqrt{\left\langle \frac{\partial \mathbf{E}^{\text{inc}}}{\partial R_k}, [\chi^{-1}\mathbb{P}(\Omega) - \mathbb{P}(\Omega)\mathbb{G}^{\text{vac}}\mathbb{P}(\Omega)]^{-1}\frac{\partial \mathbf{E}^{\text{inc}}}{\partial R_k} \right\rangle \langle \mathbf{E}^{\text{inc}}, [\chi^{-1}\mathbb{P}(\Omega) - \mathbb{P}(\Omega)\mathbb{G}^{\text{vac}}\mathbb{P}(\Omega)]^{-1}\mathbf{E}^{\text{inc}} \rangle}. \quad (4)$$

For our problem of interest, we set $|\mathbf{E}^{\text{inc}}\rangle = \mathbb{G}^{\text{vac}}|\mathbf{u}^{(\beta)}\rangle$ and identify $\mathbb{G}^{\text{sca}}(\Omega) = \mathbb{G}^{\text{vac}}[\chi^{-1}\mathbb{P}(\Omega) - \mathbb{P}(\Omega)\mathbb{G}^{\text{vac}}\mathbb{P}(\Omega)]^{-1}\mathbb{G}^{\text{vac}}$ as the scattering Green's function of the equivalent object formed by filling the entire domain Ω with the susceptibility χ [57,58]. As each $\alpha_\beta(i\xi) > 0$, the net upper bound cannot fall below the upper bound applied to each channel β, just as the net lower bound cannot fall below the per-channel lower bound. This argument also applies to integration over ξ and so (1) follows.

The above derivation has focused on forces along a given Cartesian direction k, by virtue of taking derivatives with respect to the dipole coordinate R_k. While this in itself is sufficient for yielding bounds on vertical as well as lateral forces, the result can be further generalized, such that if the dipolar basis functions $\{|\mathbf{u}^{(\beta)}\rangle\}$ (but *not* the polarizabilities, nor any properties of the macroscopic body) depend on some parameter p, upper and lower bounds on the derivative of the CP energy with respect to p follow simply by replacing the derivatives $\partial/\partial R_k$ with $\partial/\partial p$. For example, bounds on Casimir torques can be obtained by casting the dipolar basis functions in terms of a rotation angle about some axis and using that as the aforementioned parameter p.

We finally note that magnetic CP forces [61] due to nontrivial magnetic dipolar polarizabilities (which can arise even for vanishing magnetic susceptibilities [58]) can be bounded in exactly the same way, due to the same form of the CP force itself: The magnetic contribution to the force arises from replacing, in (1), the electric polarizabilities α_β (and corresponding dipolar basis functions $|\mathbf{u}^{(\beta)}\rangle$ encoding the dipolar position and principal axes) and the electric scattering Green's function $\mathbb{G}^{\text{sca}}(\Omega)$ (from filling the domain Ω) with their magnetic counterparts, namely the magnetic polarizabilities and principal axes along with the magnetic scattering Green's function from a magnetic source. The two contributions can be added to yield the total upper and lower bounds on the CP force. For the remainder of this paper, we focus only on the electric polarizabilities of dipolar particles, because magnetic contributions tend to be smaller by a factor of the square of the fine structure constant [61], but emphasize that our general method is amenable to including magnetic contributions in limits to Casimir-Polder forces.

IV. DISCUSSION

Domain monotonicity allows us to choose the largest domain enclosing any desired design, as any optimal design for attraction or repulsion in a given domain Ω cannot outdo the corresponding optimal design from a superset of that domain. This also means that while $F_k^\pm$ in (1) may be indefinite when directly evaluated, the actual bounds can be said to have a definite sign in the following way. If F_k^+ (F_k^-) is negative (positive) when filling the domain Ω with the susceptibility χ, naïvely suggesting that the maximum (minimum) possible force is attractive (repulsive), this can be circumvented by simply choosing the optimal $|\mathbf{P}\rangle$ to vanish in the domain Ω, so the actual maximum (minimum) possible force vanishes simply by virtue of the macroscopic body being absent. Therefore, we may say that F_k^+ (F_k^-) is non-negative (nonpositive), being the maximum (minimum) of zero and the given

expression in (1), and is therefore in the context of vertical CP forces a repulsive (attractive) bound.

Gratings, plates with apertures, wedges, and knife-edge geometries have all been studied in the context of CP repulsion, and experiments of interest typically consider extended nanostructured media, so we take the domain Ω to be a planar semi-infinite half-space; this choice ensures the existence of a separating plane between the dipole and the macroscopic object, in contrast to interleaved geometries [62], allowing effective repulsion through lateral forces. For this choice, $\mathbb{G}^{\text{sca}}$ of the equivalent object admits semianalytical expressions [63] (see Appendix A for more details). Additionally, the CP force and its bounds are linear functionals of the polarizabilities $\alpha_\beta(i\xi)$, and become simple linear functions if the polarizabilities are assumed to be dispersionless. Thus, for simplicity, we consistently choose the principal axes to align with the Cartesian axes, and consider $\alpha_x(0) = \alpha_y(0) = \alpha_\parallel$ and $\alpha_z(0) = \alpha_\perp$. The dipole location is taken to be $\mathbf{R} = d\mathbf{e}_z$, where d is the minimum separation of the dipole from the design domain, and the force direction of interest to lie along $\mathbf{e}_z$. This choice of polarizabilities allows us to decompose the force into parallel and perpendicular components, $F_z^\pm = g_\parallel^\pm + g_\perp^\pm \alpha_\perp/\alpha_\parallel$ for appropriate functions $g_\parallel^\pm$ and $g_\perp^\pm$ which are linearly proportional to $\alpha_\parallel$, so $F_z^\pm/\alpha_\parallel$ is an affine linear function of the polarizability ratio (similar to an aspect ratio) $\alpha_\perp/\alpha_\parallel$. These assumptions make evaluation and analysis of the CP force bounds particularly convenient.

We begin by considering a macroscopic body of dispersionless susceptibility $\chi(i\xi) = \chi_0$. This leads to the simple result that the bounds $F_z^\pm$ for this domain, as well as the CP force for a nondispersive dipole above a planar semi-infinite bulk of susceptibility χ_0, both scale as d^{-5}. Therefore, we need only consider the dependence of these bounds on χ_0 as well as the polarizability ratio $\alpha_\perp/\alpha_\parallel$. Figure 2 shows the bounds, as well as the actual attractive CP force above a planar semi-infinite bulk of susceptibility χ_0, as a function of $\alpha_\perp/\alpha_\parallel$ for multiple χ_0 (a), and as a function of χ_0 for the isotropic case $\alpha_\perp = \alpha_\parallel$ (b). As expected, for any nonzero χ_0 and $\alpha_\parallel$, the bounds and planar force (normalized by the dependence on d and $\alpha_\parallel$) attain a nonzero value for $\alpha_\perp = 0$, and increase linearly with $\alpha_\perp/\alpha_\parallel$; moreover, the bounds increase monotonically with χ_0, saturating at finite values in the perfect electrically conducting (PEC) limit $\chi_0 \to \infty$. Stunningly, the actual force is consistently within 10% of the lower bound for all χ_0 and $\alpha_\perp/\alpha_\parallel$, indicating that nanostructuring can only weakly enhance attractive CP forces in extended geometries. In (1), the first term in the summand is half of the actual force above a planar semi-infinite bulk, so the second term is crucial to making the bounds valid and tight for this domain choice. Conversely, at every χ_0 and $\alpha_\perp/\alpha_\parallel$, the upper bound is positive, suggesting that at any d and for any polarizability ratio and χ_0, there are in fact potential macroscopic geometries that can meaningfully repel dipoles. The tightness of the lower bounds indicates that these limits capture essential physics. Hence, it is fairly plausible that tailored macroscopic geometries approaching the upper bound do exist. It is also worth mentioning that in the few geometries where repulsion is predicted for strongly anisotropic dipoles, it is prohibited for isotropic dipoles, but our upper bounds do not rule out the existence of other repulsive geometries even
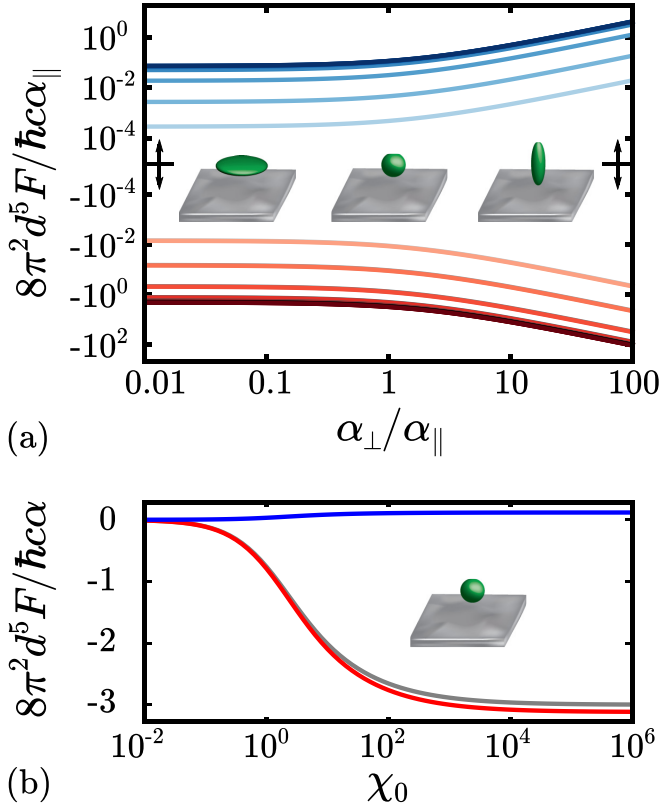
(a)

(b)

FIG. 2. Material and anisotropy dependence of bounds on Casimir-Polder forces. (a) Upper and lower bounds to the CP force (blue and red lines, respectively, in the upper or lower parts of the plot) on a nondispersive anisotropic dipole of parallel and perpendicular polarizabilities $\alpha_\parallel$ and $\alpha_\perp$, above a planar semi-infinite half-space domain, along with the actual force above a planar semi-infinite bulk (gray lines, nearly overlapping with red lines in the lower part of the plot), normalized to $\hbar c \alpha_\parallel / 8\pi^2 d^5$ for separation d, as a function of $\alpha_\perp / \alpha_\parallel$. The macroscopic susceptibility χ_0 is nondispersive and increases logarithmically from 10^{-2} to 10^6 (going from lighter to darker shades upward in the upper part of the plot or downward in the lower part of the plot). (b) Same as panel (a) but plotted against χ_0 for the isotropic case $\alpha_\perp = \alpha_\parallel$.

for isotropic dipoles. Finally, we point out that the magnitude of the upper bounds are consistently more than an order of magnitude smaller than the magnitude of the lower bounds.

Next, we relax the assumption that $\chi(i\xi)$ is nondispersive, and consider the particular case of a gold medium, for which $\chi(i\xi) = \omega_p^2/(\xi^2 + \gamma\xi)$ for $\omega_p = 1.37 \times 10^{16}$ rad/s and $\gamma = 5.32 \times 10^{13}$ rad/s [64]. For simplicity, we continue to neglect dispersion in $\alpha_\parallel$ and $\alpha_\perp$, so the linear scaling of the bounds with $\alpha_\parallel$ and affine linear scaling with $\alpha_\perp / \alpha_\parallel$ are preserved. The introduction of dispersion means that the bounds no longer scale uniformly as d^{-5}: As seen in Fig. 3, the bounds transition from the nonretarded scaling of d^{-4} toward d^{-5} as the separation increases. The linear increase in the bounds with $\alpha_\perp / \alpha_\parallel$ is also clear. More importantly, while more than an order of magnitude smaller than the lower bounds, for a dispersive metal like gold the possibility of repulsion is still not ruled out as the upper bounds remain positive for all d and $\alpha_\perp / \alpha_\parallel$. For attraction, the actual forces produce
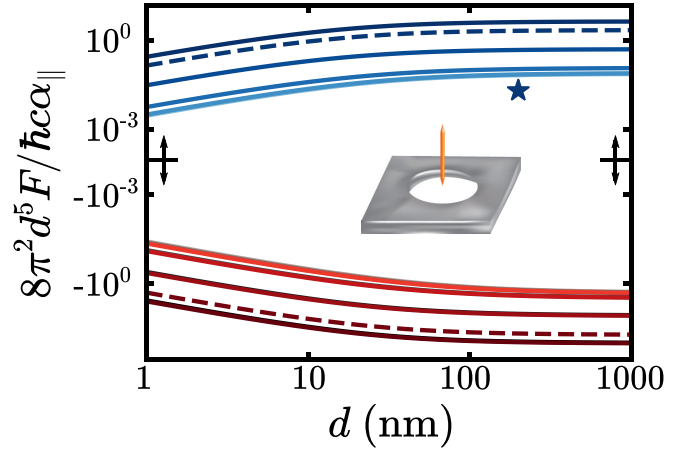

FIG. 3. Distance dependence of bounds on Casimir-Polder forces for gold nanostructures. Repulsive and attractive bounds on CP forces as in Fig. 2 but with the macroscopic susceptibility χ corresponding to that of gold and $\alpha_\perp / \alpha_\parallel$ increasing logarithmically from 10^{-2} to 10^2 (going from lighter to darker shades upward in the upper part of the plot or downward in the lower part of the plot). Also shown is the CP force on a gold needle above a gold plate with a circular aperture from Ref. [49] (dark blue star), corresponding to a static anisotropic polarizability ratio $\alpha_\perp / \alpha_\parallel \approx 51.1$ at $d = 200$ nm; bounds for $\alpha_\perp / \alpha_\parallel = 50$ are marked in dashed lines.

from the planar geometry are again within 10% of the corresponding lower bounds for all d and $\alpha_\perp / \alpha_\parallel$, demonstrating that these results are not simply artifacts of a nondispersive χ. We further compare the bounds for gold to the actual repulsive force by a gold plate with a circular aperture upon a gold nanorod at a center-to-center separation of $d = 200$ nm, approximating the nanorod as an ellipsoid with the same major and minor axes (320 and 20 nm, respectively) using the anisotropic Clausius-Mossotti form of the polarizability [65]. The dipolar approximation may not be valid given that the separation is smaller than the major axis length, but we use this simply as a heuristic to make qualitative comparisons to our bounds. Approximating the nanorod as a PEC, the polarizability ratio is $\alpha_\perp / \alpha_\parallel \approx 51.1$: For that ratio and d, the actual force [49] is more than two orders of magnitude smaller than the upper bound, strongly suggesting that macroscopic geometries optimized for CP repulsion may look quite different from prior proposed geometries. Finally, we briefly note comparisons to other material models. The bounds show qualitatively similar behaviors for polar dielectrics like undoped silicon as for metals like gold, though those of silicon are smaller than their counterparts for gold. Also, the differences between gold evaluated using this Drude susceptibility versus a plasma susceptibility are negligible for the actual forces on a dipolar particle above a semi-infinite slab, as well as for the corresponding bounds in such a domain, at zero or room temperatures (consistent with prior findings to which we compare [49]). Both of these results are further discussed in Appendix C.

In summary, we have derived bounds for the CP force on a general anisotropic dipolar body by a macroscopic body of susceptibility χ enclosed within a prescribed domain, and have evaluated these bounds specifically for a planar

semi-infinite half-space domain. The lower bounds are nearly achieved by the typical geometry of a dipole above a uniform planar body, whereas existing predictions of repulsive CP forces in geometries involving conductors with sharp edges fall nearly two orders of magnitude below the limits on repulsion. We expect that, similar to other nanophotonic phenomena like local density of states modifications and radiative heat transfer, optimal structures for attraction or repulsion found through brute-force techniques such as topology optimization [66–68] will look very different from the high-symmetry geometries proposed thus far. In particular, the tightness of the lower (attractive) bounds for known structures suggests that appropriately designed structures, aided by advances in computational design [66–68] and fabrication [68,69] in nanophotonics, may indeed approach the upper bounds and yield *measurable* repulsive CP forces even for relatively *isotropic* dipoles like Rydberg atoms, in contrast to existing designs [1,2,44,49,50], yielding much greater control over ultracold atoms, molecules, and dipolar nanoparticles. Additionally, we point out that a specific structure optimized for repulsion from a dipole at a given distance will attract dipoles when that distance is increased beyond a certain point, but for such changes in distance, redoing optimization for repulsion may yield different structures. Though our results focused on the force normal to the plane separating the dipolar and extended bodies, (1) can be employed to bound lateral forces and torques, the subject of much recent interest [18,25,35,70–74], as well as forces involving compact objects.

APPENDIX A: GREEN'S FUNCTION EXPRESSIONS IN REAL SPACE

We define $\mathbb{G}^{\mathrm{vac}}$ as the tensor operator that is the inverse of the Maxwell operator, satisfying $\{[\nabla \times (\nabla \times)] - (\omega/c)^2 \mathbb{I}\}\mathbb{G}^{\mathrm{vac}}(\omega, \mathbf{x}, \mathbf{x}') = (\omega/c)^2 \mathbb{I} \delta^3(\mathbf{x} - \mathbf{x}')$. In position space and evaluating at $\omega = i\xi$, this yields the expression $\mathbb{G}^{\mathrm{vac}}(i\xi, \mathbf{x}, \mathbf{x}') = [\nabla \otimes \nabla - (\xi/c)^2](e^{-\xi|\mathbf{x}-\mathbf{x}'|/c}/4\pi |\mathbf{x} - \mathbf{x}'|)$.

The scattering Green's function at $\omega = i\xi$ in the vacuum region above a uniform planar semi-infinite half-space of susceptibility χ is [63]

$$\mathbb{G}^{\mathrm{sca}}(i\xi, \mathbf{x}, \mathbf{x}') = \frac{1}{2} \int_{-\infty}^{\infty} \int_{-\infty}^{\infty} [\mathbb{M}^{\mathrm{s}}(i\xi, \mathbf{k}) + \mathbb{M}^{\mathrm{p}}(i\xi, \mathbf{k})]$$
$$\times e^{i[k_x(x-x')+k_y(y-y')]-\kappa_z(z+z')} \frac{dk_x dk_y}{(2\pi)^2} \quad \text{(A1)}$$

defined in terms of the Cartesian tensors

$$\mathbb{M}^{\mathrm{s}}(i\xi, \mathbf{k}) = -\frac{\xi^2 r^{\mathrm{s}}(i\xi, k)}{c^2 \kappa_z k^2} \begin{bmatrix} k_y^2 & -k_x k_y & 0 \\ -k_x k_y & k_x^2 & 0 \\ 0 & 0 & 0 \end{bmatrix}, \quad \text{(A2)}$$

$$\mathbb{M}^{\mathrm{p}}(i\xi, \mathbf{k}) = \frac{r^{\mathrm{p}}(i\xi, k)}{k^2} \begin{bmatrix} \kappa_z k_x^2 & \kappa_z k_x k_y & -ik^2 k_x \\ \kappa_z k_x k_y & \kappa_z k_y^2 & -ik^2 k_y \\ ik^2 k_x & ik^2 k_y & k^4/\kappa_z \end{bmatrix}, \quad \text{(A3)}$$

which are in turn defined in terms of $\mathbf{k} = k_x \mathbf{e}_x + k_y \mathbf{e}_y$, $k = |\mathbf{k}|$, $\kappa_z = \sqrt{(\xi/c)^2 + k^2}$, and the Fresnel reflection coefficients

$$r^{\mathrm{s}}(i\xi, k) = \frac{\sqrt{(\xi/c)^2 + k^2} - \sqrt{(1+\chi)(\xi/c)^2 + k^2}}{\sqrt{(\xi/c)^2 + k^2} + \sqrt{(1+\chi)(\xi/c)^2 + k^2}}, \quad \text{(A4)}$$

$$r^{\mathrm{p}}(i\xi, k) = \frac{(1+\chi)\sqrt{(\xi/c)^2 + k^2} - \sqrt{(1+\chi)(\xi/c)^2 + k^2}}{(1+\chi)\sqrt{(\xi/c)^2 + k^2} + \sqrt{(1+\chi)(\xi/c)^2 + k^2}} \quad \text{(A5)}$$

at $\omega = i\xi$.

APPENDIX B: CASIMIR-POLDER FORCE DERIVATION

We start our derivation of the (zero-temperature) Casimir-Polder force between a dipole of susceptibility $\mathbb{V}_{\mathrm{dip}}$ and a macroscopic body of susceptibility $\mathbb{V}$ from the exact expression for the (zero-temperature) Casimir force between the two bodies. This force is written as [57]

$$F_k = -\frac{\partial}{\partial R_k} \hbar \int_0^{\infty} \ln(\det[\mathbb{I} - \mathbb{T}_{\mathrm{dip}} \mathbb{G}^{\mathrm{vac}} \mathbb{T} \mathbb{G}^{\mathrm{vac}}]) \frac{d\xi}{2\pi}, \quad \text{(B1)}$$

where $\mathbb{T} = (\mathbb{V}^{-1} - \mathbb{G}^{\mathrm{vac}})^{-1} = (\mathbb{I} - \mathbb{V}\mathbb{G}^{\mathrm{vac}})^{-1}\mathbb{V}$ and likewise $\mathbb{T}_{\mathrm{dip}} = (\mathbb{V}_{\mathrm{dip}}^{-1} - \mathbb{G}^{\mathrm{vac}})^{-1} = (\mathbb{I} - \mathbb{V}_{\mathrm{dip}}\mathbb{G}^{\mathrm{vac}})^{-1}\mathbb{V}_{\mathrm{dip}}$, and where all quantities are evaluated at $\omega = i\xi$. Here, $\mathbf{R}$ is taken to denote the dipole location, and $\mathbb{T}_{\mathrm{dip}}$ is the only quantity that depends on it.

The force may be rewritten as

$$F_k = \hbar \int_0^{\infty} \mathrm{Tr}\left[\mathbb{G}^{\mathrm{vac}} \mathbb{T} \mathbb{G}^{\mathrm{vac}} (\mathbb{I} - \mathbb{T}_{\mathrm{dip}} \mathbb{G}^{\mathrm{vac}} \mathbb{T} \mathbb{G}^{\mathrm{vac}})^{-1} \right.$$
$$\left. \times \frac{\partial}{\partial R_k} \mathbb{T}_{\mathrm{dip}} \right] \frac{d\xi}{2\pi} \quad \text{(B2)}$$

after applying the derivative to the integrand. At this point, it is assumed that the dipole is small enough compared to the macroscopic body that multiple scattering effects may be neglected, though multiple scattering within each object is not. This has the effect of making the replacement $(\mathbb{I} - \mathbb{T}_{\mathrm{dip}}\mathbb{G}^{\mathrm{vac}}\mathbb{T}\mathbb{G}^{\mathrm{vac}})^{-1} \to \mathbb{I}$. Furthermore, we expand the dipolar response, including local field effects, along its principal axes as $\mathbb{T}_{\mathrm{dip}} = \sum_{\beta} \alpha_{\beta} |\mathbf{u}^{(\beta)}\rangle\langle\mathbf{u}^{(\beta)}|$, where each $\alpha_{\beta}(i\xi) > 0$ is a principal polarizability, while $\mathbf{u}^{(\beta)}(\mathbf{x}) = \mathbf{n}_{\beta}\delta^3(\mathbf{x} - \mathbf{R})$ corresponds to a localized basis function at $\mathbf{R}$ along principal axis $\mathbf{n}_{\beta}$. Finally, using the cyclic properties of the trace and the independence of $\mathbb{G}^{\mathrm{vac}}$, $\mathbb{T}$, and α_{β} from $\mathbf{R}$ yields the Casimir-Polder force

$$F_k = \frac{\hbar}{2\pi} \int_0^{\infty} \sum_{\beta} \alpha_{\beta} \frac{\partial}{\partial R_k} \langle \mathbf{u}^{(\beta)}, \mathbb{G}^{\mathrm{vac}} \mathbb{T} \mathbb{G}^{\mathrm{vac}} \mathbf{u}^{(\beta)} \rangle \, d\xi \quad \text{(B3)}$$
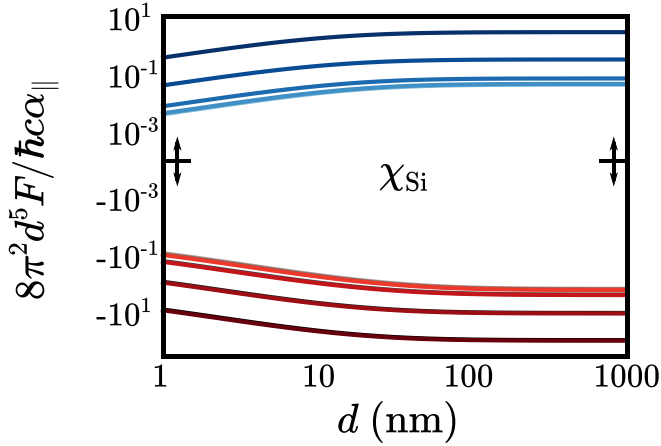
exactly as in the main text.

FIG. 4. Distance dependence of bounds on Casimir-Polder forces for silicon nanostructures. Repulsive and attractive bounds on CP forces (blue and red lines, respectively, in the upper or lower part of the plot) and actual force (gray lines, nearly overlapping with red lines in the lower part of the plot) for the macroscopic susceptibility χ corresponding to that of silicon and $\alpha_\perp/\alpha_\parallel$ increasing logarithmically from 10^{-2} to 10^2 (going from lighter to darker shades upward in the upper part of the plot or downward in the lower part of the plot).

APPENDIX C: FURTHER RESULTS FOR EVALUATIONS OF BOUNDS

We provide more results for evaluations of our bounds, starting with undoped silicon at zero temperature in Fig. 4. The dispersion of intrinsic silicon is given by [75] $\chi(i\xi) = \epsilon(\infty) - 1 + \frac{\epsilon(0) + \epsilon(\infty)}{1 + \xi^2/\omega_0^2}$, where $\epsilon(0) = 11.87$, $\epsilon(\infty) = 1.035$, and $\omega_0 = 6.6 \times 10^{15}$ rad/s. From this, it is clear that the bounds for undoped silicon qualitatively behave like those for gold, though those of silicon are smaller than their counterparts for gold.

Next, we provide further comparisons of the evaluations of the bounds for gold in the main text to cases where the temperature is varied or a different model is used. In particular, at zero temperature, the expressions for the actual force and bounds in the main text hold. If the actual CP force or its bounds at zero temperature are written as $F(0) = \hbar \int_0^\infty f(i\xi) \frac{d\xi}{2\pi}$ for the corresponding integrand $f(i\xi)$, then the corresponding quantities for temperature $T > 0$ are $F(T) = k_B T \sum_{n=0}^\infty{}' f(i\xi_n)$ where the Matsubara frequencies are $\xi_n = 2\pi k_B T n/\hbar$, and the prime on the summation implies a prefactor of $1/2$ for the contribution at $n = 0$; we particularly consider room temperature, namely $T = 300$ K. We further compare results from the Drude model, for which $\chi(i\xi) = \omega_p^2/(\xi^2 + \gamma\xi)$ for $\omega_p = 1.37 \times 10^{16}$ rad/s and $\gamma = 5.32 \times 10^{13}$ rad/s, to those of the plasma model, setting $\gamma \to 0$ in the aforementioned expression. As is clear from Fig. 5,
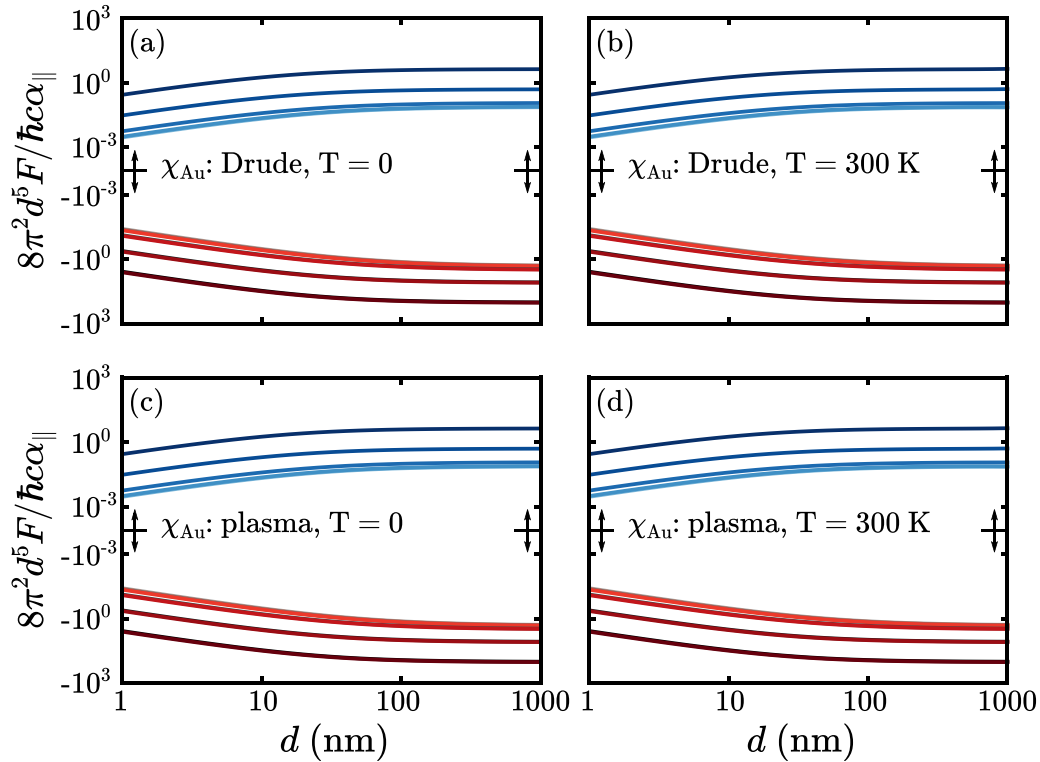

FIG. 5. Distance dependence of bounds on Casimir-Polder forces for gold nanostructures: dependence on model and temperature. Repulsive and attractive bounds on CP forces (blue and red lines, respectively in the upper or lower part of the plots) and actual force (gray lines, nearly overlapping with red lines in the lower part of the plots) with the macroscopic susceptibility χ corresponding to that of gold and $\alpha_\perp/\alpha_\parallel$ increasing logarithmically from 10^{-2} to 10^2 (going from lighter to darker shades upward in the upper part of the plots or downward in the lower part of the plots), for the Drude model at zero (a) or room (b) temperatures. [(c), (d)] Same as panels (a) and (b), respectively, using the plasma model instead.
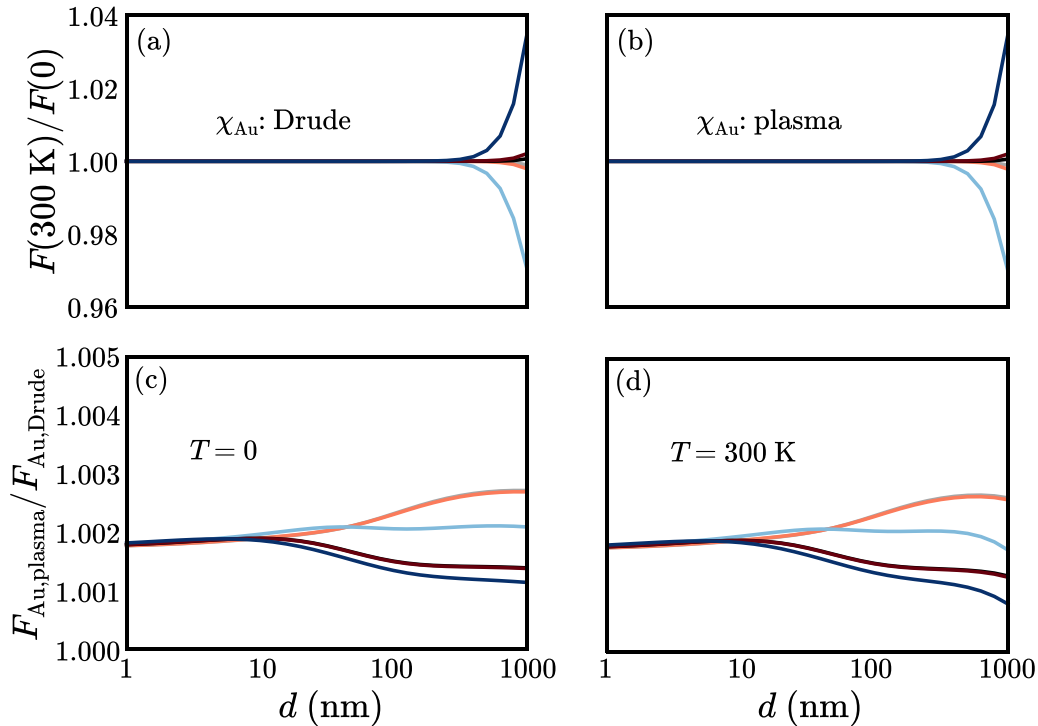
FIG. 6. Ratios of bounds on Casimir-Polder forces for gold nanostructures. Ratios of corresponding repulsive and attractive bounds on CP forces (blue and red lines) and actual forces (gray lines, nearly overlapping with red lines), with the macroscopic susceptibility χ corresponding to that of gold and $\alpha_\perp/\alpha_\parallel$ increasing logarithmically from 10^{-2} to 10^2 (lighter to darker shades). For panels (a) and (b), ratios are of $\frac{F(300\,\mathrm{K})}{F(0)}$ for the Drude (a) or plasma (b) models: For both plots, from top to bottom, the top-most dark blue curve is the repulsive bound ratio for $\alpha_\perp/\alpha_\parallel = 10^2$, the next dark red curve is the attractive bound ratio for $\alpha_\perp/\alpha_\parallel = 10^2$, the following light red curve is the attractive bound ratio for $\alpha_\perp/\alpha_\parallel = 10^{-2}$, and the bottom-most light blue curve is the repulsive bound ratio for $\alpha_\perp/\alpha_\parallel = 10^{-2}$. For panels (c) and (d), ratios are of $\frac{F_{\mathrm{Au,plasma}}}{F_{\mathrm{Au,Drude}}}$, for zero (c) or room (d) temperatures: For both plots, from top to bottom, the top-most light red curve is the attractive bound ratio for $\alpha_\perp/\alpha_\parallel = 10^{-2}$, the next light blue curve is the repulsive bound ratio for $\alpha_\perp/\alpha_\parallel = 10^{-2}$, the following dark red curve is the attractive bound ratio for $\alpha_\perp/\alpha_\parallel = 10^2$, and the bottom-most dark blue curve is the repulsive bound ratio for $\alpha_\perp/\alpha_\parallel = 10^2$.

the corresponding actual CP forces and bounds are all quite close to each other in each case. This is further made clear in Fig. 6 by the fact that for each material model, the ratios $\frac{F(300\,\mathrm{K})}{F(0)}$ do not significantly stray from 1 even at $d = 1\,\mu$m, and the same is true of the ratios $\frac{F_{\mathrm{Au,plasma}}}{F_{\mathrm{Au,Drude}}}$ for each temperature.

Ultimately, this means that our bounds on CP forces when the macroscopic body is made of gold, just like the actual force on a dipole above a semi-infinite gold half-space, do not depend strongly on the particular susceptibility model (Drude versus plasma), nor on the temperature. The contrast between this, in conjunction with prior theoretical work [49]

showing minimal differences in predictions of the CP force on a vertical needle by a plate with a hole using the Drude or plasma models, versus the more significant discrepancies in predictions of the forces between parallel semi-infinite planar slabs, which is the subject of ongoing experimental controversy [18,76–78], suggests that the presence and magnitude of such discrepancies may in fact be much more dependent on specific geometries. In any case, this paper intends not to specifically comment on this particular controversy but to more generally present bounds that can be applicable at any temperature and any appropriate local, homogeneous, isotropic model of material dispersion.

[1] S. Y. Buhmann, *Dispersion Forces I: Macroscopic Quantum Electrodynamics and Ground-State Casimir, Casimir-Polder, and van der Waals Forces* (Springer, Berlin, 2012).

[2] S. Y. Buhmann, *Dispersion Forces II: Many-Body Effects, Excited Atoms, Finite Temperature, and Quantum Friction* (Springer, Berlin, 2012).

[3] F. Intravaia, C. Henkel, and M. Antezza, Fluctuation-induced forces between atoms and surfaces: The Casimir-Polder interaction, in *Casimir Physics*, edited by D. Dalvit, P.

Milonni, D. Roberts, and F. da Rosa (Springer, Berlin, 2011), pp. 345–391.

[4] M. DeKieviet, U. D. Jentschura, and G. Łach, Modern experiments on atom-surface Casimir physics, in *Casimir Physics*, edited by D. Dalvit, P. Milonni, D. Roberts, and F. da Rosa (Springer, Berlin, 2011), pp. 393–418.

[5] G. S. Agarwal, Quantum electrodynamics in the presence of dielectrics and conductors. II. Theory of dispersion forces, Phys. Rev. A **11**, 243 (1975).

[6] P. S. Venkataram, J. Hermann, A. Tkatchenko, and A. W. Rodriguez, Unifying Microscopic and Continuum Treatments of Van Der Waals and Casimir Interactions, Phys. Rev. Lett. **118**, 266802 (2017).

[7] P. Barcellona, R. Passante, L. Rizzuto, and S. Y. Buhmann, Dynamical Casimir-Polder interaction between a chiral molecule and a surface, Phys. Rev. A **93**, 032508 (2016).

[8] L. M. Woods, D. A. R. Dalvit, A. Tkatchenko, P. Rodriguez-Lopez, A. W. Rodriguez, and R. Podgornik, Materials perspective on Casimir and van der Waals interactions, Rev. Mod. Phys. **88**, 045003 (2016).

[9] A. Tkatchenko, R. A. DiStasio, Jr., R. Car, and M. Scheffler, Accurate and Efficient Method for Many-Body Van Der Waals Interactions, Phys. Rev. Lett. **108**, 236402 (2012).

[10] M. Chattopadhyaya, J. Hermann, I. Poltavsky, and A. Tkatchenko, Tuning intermolecular interactions with nanostructured environments, Chem. Mater. **29**, 2452 (2017).

[11] J. Hermann, R. A. DiStasio, and A. Tkatchenko, First-principles models for van der Waals interactions in molecules and materials: Concepts, theory, and applications, Chem. Rev. **117**, 4714 (2017).

[12] C. Wagner, N. Fournier, V. G. Ruiz, C. Li, K. Müllen, M. Rohlfing, A. Tkatchenko, R. Temirov, and F. S. Tautz, Non-additivity of molecule-surface van der Waals potentials from force measurements, Nat. Commun. **5**, 5568 (2014).

[13] P. Loskill, J. Puthoff, M. Wilkinson, K. Mecke, K. Jacobs, and K. Autumn, Macroscale adhesion of gecko setae reflects nanoscale differences in subsurface composition, J. R. Soc. Int. **10**, 20120587 (2013).

[14] S. Tsoi, P. Dev, A. L. Friedman, R. Stine, J. T. Robinson, T. L. Reinecke, and P. E. Sheehan, Van der Waals screening by single-layer graphene and molybdenum disulfide, ACS Nano **8**, 12410 (2014).

[15] G. A. Rance, D. H. Marsh, S. J. Bourne, T. J. Reade, and A. N. Khlobystov, Van der Waals interactions between nanotubes and nanoparticles for controlled assembly of composite nanostructures, ACS Nano **4**, 4920 (2010).

[16] C. A. Silvera Batista, R. G. Larson, and N. A. Kotov, Non-additivity of nanoparticle interactions, Science **350**, 1242477 (2015).

[17] H. Bender, C. Stehle, C. Zimmermann, S. Slama, J. Fiedler, S. Scheel, S. Y. Buhmann, and V. N. Marachevsky, Probing Atom-Surface Interactions by Diffraction of Bose-Einstein Condensates, Phys. Rev. X **4**, 011029 (2014).

[18] G. L. Klimchitskaya, U. Mohideen, and V. M. Mostepanenko, The Casimir force between real materials: Experiment and theory, Rev. Mod. Phys. **81**, 1827 (2009).

[19] A. A. Banishev, H. Wen, J. Xu, R. K. Kawakami, G. L. Klimchitskaya, V. M. Mostepanenko, and U. Mohideen, Measuring the Casimir force gradient from graphene on a SiO_2 substrate, Phys. Rev. B **87**, 205433 (2013).

[20] A. Sushkov, W. Kim, D. Dalvit, and S. Lamoreaux, Observation of the thermal Casimir force, Nat. Phys. **7**, 230 (2011).

[21] G. L. Klimchitskaya and V. M. Mostepanenko, Comparison of hydrodynamic model of graphene with recent experiment on measuring the Casimir interaction, Phys. Rev. B **91**, 045412 (2015).

[22] J. L. Garrett, D. A. T. Somers, and J. N. Munday, Measurement of the Casimir Force Between two Spheres, Phys. Rev. Lett. **120**, 040401 (2018).

[23] R. Zhao, L. Li, S. Yang, W. Bao, Y. Xia, P. Ashby, Y. Wang, and X. Zhang, Stable Casimir equilibria and quantum trapping, Science **364**, 984 (2019).

[24] J. N. Munday, F. Capasso, and V. A. Parsegian, Measured long-range repulsive Casimir-Lifshitz forces, Nature (London) **457**, 170 (2009).

[25] F. Chen, U. Mohideen, G. L. Klimchitskaya, and V. M. Mostepanenko, Demonstration of the Lateral Casimir Force, Phys. Rev. Lett. **88**, 101801 (2002).

[26] L. Tang, M. Wang, C. Ng, M. Nikolic, C. T. Chan, A. W. Rodriguez, and H. B. Chan, Measurement of non-monotonic Casimir forces between silicon nanostructures, Nat. Photon. **11**, 97 (2017).

[27] A. W. Rodriguez, F. Capasso, and S. G. Johnson, The Casimir effect in microstructured geometries, Nat. Photon. **5**, 211 (2011).

[28] E. Zaremba and W. Kohn, Van der waals interaction between an atom and a solid surface, Phys. Rev. B **13**, 2270 (1976).

[29] A. Tkatchenko, Current understanding of van der Waals effects in realistic materials, Adv. Functional Mater. **25**, 2054 (2015).

[30] D. Langbein, Theory of van der Waals attraction, in *Springer Tracts in Modern Physics* (Springer, Berlin, 1974), pp. 1–139.

[31] A. M. Reilly and A. Tkatchenko, Role of Dispersion Interactions in the Polymorphism and Entropic Stabilization of the Aspirin Crystal, Phys. Rev. Lett. **113**, 055701 (2014).

[32] J. Hoja, A. M. Reilly, and A. Tkatchenko, First-principles modeling of molecular crystals: Structures and stabilities, temperature and pressure, Wiley Interdisc. Rev.: Comp. Mol. Sci. **7**, e1294 (2017).

[33] A. Ambrosetti, N. Ferri, R. A. DiStasio, Jr., and A. Tkatchenko, Wavelike charge density fluctuations and van der Waals interactions at the nanoscale, Science **351**, 1171 (2016).

[34] R. H. French, V. A. Parsegian, R. Podgornik, R. F. Rajter, A. Jagota, J. Luo, D. Asthagiri, M. K. Chaudhury, Y.-M. Chiang, S. Granick, S. Kalinin, M. Kardar, R. Kjellander, D. C. Langreth, J. Lewis, S. Lustig, D. Wesolowski, J. S. Wettlaufer, W.-Y. Ching, M. Finnis, F. Houlihan, O. A. von Lilienfeld, C. J. van Oss, and T. Zemb, Long range interactions in nanoscale science, Rev. Mod. Phys. **82**, 1887 (2010).

[35] F. Capasso, J. N. Munday, D. Iannuzzi, and H. B. Chan, Casimir forces and quantum electrodynamical torques: Physics and nanomechanics, IEEE J. Sel. Topics Quantum Electr. **13**, 400 (2007).

[36] M. Miri and R. Golestanian, A frustrated nanomechanical device powered by the lateral casimir force, Appl. Phys. Lett. **92**, 113103 (2008).

[37] C. Genet, A. Lambrecht, and S. Reynaud, The Casimir effect in the nanoworld, Eur. Phys. J. Special Top. **160**, 183 (2008).

[38] S. Y. Buhmann, S. Scheel, S. A. Ellingsen, K. Hornberger, and A. Jacob, Casimir-Polder interaction of fullerene molecules with surfaces, Phys. Rev. A **85**, 042513 (2012).

[39] H. Safari, S. Y. Buhmann, D.-G. Welsch, and H. T. Dung, Body-assisted van der Waals interaction between two atoms, Phys. Rev. A **74**, 042101 (2006).

[40] S. Y. Buhmann, V. N. Marachevsky, and S. Scheel, Impact of anisotropy on the interaction of an atom with a one-dimensional nano-grating, Int. J. Mod. Phys. A **31**, 1641029 (2016).

[41] I. E. Dzyaloshinskii, E. M. Lifshitz, and L. P. Pitaevskii, The general theory of van der Waals forces, Adv. Phys. **10**, 165 (1961).

[42] K. A. Milton, E. K. Abalo, P. Parashar, N. Pourtolami, I. Brevik, and S. Å. Ellingsen, Repulsive Casimir and Casimir-Polder forces, J. Phys. A: Math. Theor. **45**, 374006 (2012).

[43] I. Pirozhenko and A. Lambrecht, Repulsive Casimir forces and the role of surface modes, Phys. Rev. A **80**, 042510 (2009).

[44] K. V. Shajesh and M. Schaden, Repulsive long-range forces between anisotropic atoms and dielectrics, Phys. Rev. A **85**, 012523 (2012).

[45] K. A. Milton, P. Parashar, N. Pourtolami, and I. Brevik, Casimir-Polder repulsion: Polarizable atoms, cylinders, spheres, and ellipsoids, Phys. Rev. D **85**, 025008 (2012).

[46] L. Rosa and A. Lambrecht, Repulsive Casimir force: Sufficient conditions, Phys. Rev. D **82**, 065025 (2010).

[47] I. G. Pirozhenko and A. Lambrecht, Casimir repulsion and metamaterials, J. Phys. A: Math. Theor. **41**, 164015 (2008).

[48] A. Lambrecht and I. G. Pirozhenko, Casimir force between dissimilar mirrors and the role of the surface plasmons, Phys. Rev. A **78**, 062102 (2008).

[49] M. Levin, A. P. McCauley, A. W. Rodriguez, M. T. H. Reid, and S. G. Johnson, Casimir Repulsion Between Metallic Objects in Vacuum, Phys. Rev. Lett. **105**, 090403 (2010).

[50] C. Eberlein and R. Zietal, Casimir-Polder interaction between a polarizable particle and a plate with a hole, Phys. Rev. A **83**, 052514 (2011).

[51] M. F. Maghrebi, Diagrammatic expansion of the Casimir energy in multiple reflections: Theory and applications, Phys. Rev. D **83**, 045004 (2011).

[52] K. A. Milton, E. K. Abalo, P. Parashar, N. Pourtolami, I. Brevik, and S. A. Ellingsen, Casimir-Polder repulsion near edges: Wedge apex and a screen with an aperture, Phys. Rev. A **83**, 062507 (2011).

[53] O. Kenneth and I. Klich, Opposites Attract: A Theorem About the Casimir Force, Phys. Rev. Lett. **97**, 160401 (2006).

[54] S. J. Rahi, M. Kardar, and T. Emig, Constraints on Stable Equilibria with Fluctuation-Induced (Casimir) Forces, Phys. Rev. Lett. **105**, 070404 (2010).

[55] C. Henkel and K. Joulain, Casimir force between designed materials: What is possible and what not, Europhys. Lett. **72**, 929 (2005).

[56] A. Lambrecht, M.-T. Jaekel, and S. Reynaud, The Casimir force for passive mirrors, Phys. Lett. A **225**, 188 (1997).

[57] S. J. Rahi, T. Emig, N. Graham, R. L. Jaffe, and M. Kardar, Scattering theory approach to electrodynamic Casimir forces, Phys. Rev. D **80**, 085021 (2009).

[58] M. Krüger, G. Bimonte, T. Emig, and M. Kardar, Trace formulas for nonequilibrium Casimir interactions, heat radiation, and heat transfer for arbitrary objects, Phys. Rev. B **86**, 115423 (2012).

[59] B. A. Lippmann and J. Schwinger, Variational principles for scattering processes. I, Phys. Rev. **79**, 469 (1950).

[60] S. Molesky, P. Chao, and A. W. Rodriguez, $\mathbb{T}$-operator bounds on electromagnetic power transfer: Application to far-field cross sections, arXiv:2001.11531 (2020).

[61] D. Reiche, K. Busch, and F. Intravaia, Quantum thermodynamics of overdamped modes in local and spatially dispersive materials, Phys. Rev. A **101**, 012506 (2020).

[62] A. W. Rodriguez, J. D. Joannopoulos, and S. G. Johnson, Repulsive and attractive Casimir forces in a glide-symmetric geometry, Phys. Rev. A **77**, 062107 (2008).

[63] L. Novotny and B. Hecht, in *Principles of Nano-optics* (Cambridge University Press, Cambridge, UK, 2006), pp. 335–362.

[64] M. T. H. Reid, J. White, and S. G. Johnson, Fluctuating surface currents: An algorithm for efficient prediction of Casimir interactions among arbitrary materials in arbitrary geometries, Phys. Rev. A **88**, 022514 (2013).

[65] C. F. Bohren and D. R. Huffman, Particles small compared with the wavelength, in *Absorption and Scattering of Light by Small Particles* (John Wiley & Sons, New York, 2007), Chap. 5, pp. 130–157.

[66] W. Jin, S. Molesky, Z. Lin, and A. W. Rodriguez, Material scaling and frequency-selective enhancement of near-field radiative heat transfer for lossy metals in two dimensions via inverse design, Phys. Rev. B **99**, 041403(R) (2019).

[67] W. Jin, S. Molesky, Z. Lin, K.-M. C. Fu, and A. W. Rodriguez, Inverse design of compact multimode cavity couplers, Opt. Express **26**, 26713 (2018).

[68] S. Molesky, Z. Lin, A. Y. Piggott, W. Jin, J. Vucković, and A. W. Rodriguez, Inverse design in nanophotonics, Nat. Photon. **12**, 659 (2018).

[69] A. D. Logan, M. Gould, E. R. Schmidgall, K. Hestroffer, Z. Lin, W. Jin, A. Majumdar, F. Hatami, A. W. Rodriguez, and K.-M. C. Fu, 400%/W second harmonic conversion efficiency in 14 μm-diameter gallium phosphide-on-oxide resonators, Opt. Express **26**, 33687 (2018).

[70] T. Emig, A. Hanke, R. Golestanian, and M. Kardar, Normal and lateral Casimir forces between deformed plates, Phys. Rev. A **67**, 022114 (2003).

[71] G. L. Klimchitskaya, Normal and lateral Casimir force: Advances and prospects, J. Phys.: Conf. Series **258**, 012001 (2010).

[72] A. Manjavacas, F. J. Rodríguez-Fortuño, F. J. García de Abajo, and A. V. Zayats, Lateral Casimir Force on a Rotating Particle Near a Planar Surface, Phys. Rev. Lett. **118**, 133605 (2017).

[73] M. Antezza, H. B. Chan, B. Guizal, V. N. Marachevsky, R. Messina, and M. Wang, Giant Casimir Torque Between Rotated Gratings and the $\theta = 0$ Anomaly, Phys. Rev. Lett. **124**, 013903 (2020).

[74] D. A. Somers, J. L. Garrett, K. J. Palm, and J. N. Munday, Measurement of the Casimir torque, Nature (London) **564**, 386 (2018).

[75] A. Lambrecht, I. Pirozhenko, L. Duraffourg, and P. Andreucci, The Casimir effect for silicon and gold slabs, Europhys. Lett. **77**, 44006 (2007).

[76] K. A. Milton, The Casimir effect: Recent controversies and progress, J. Phys. A: Math. Gen. **37**, R209 (2004).

[77] B. E. Sernelius, Finite-temperature Casimir force between metal plates: Full inclusion of spatial dispersion resolves a long-standing controversy, J. Phys. A: Math. Gen. **39**, 6741 (2006).

[78] G. Bimonte, D. López, and R. S. Decca, Isoelectronic determination of the thermal Casimir force, Phys. Rev. B **93**, 184434 (2016).